Published in final edited form as:
Science. 2012 December 21; 338(6114): 1631–1634. doi:10.1126/science.1227270.

Organization of the Influenza Virus Replication Machinery

Arne Moeller[1,†], **Robert N. Kirchdoerfer**[2,†], **Clinton S. Potter**[1], **Bridget Carragher**[1,*], and **Ian A. Wilson**[2,3,*]

[1]National Resource for Automated Molecular Microscopy, Department of Cell Biology, La Jolla, California 92037, United States

[2]Department of Molecular Biology La Jolla, California 92037, United States

[3]The Skaggs Institute for Chemical Biology, The Scripps Research Institute, La Jolla, California 92037, United States

Abstract

Influenza virus ribonucleoprotein complexes (RNPs) are central to the viral life cycle and in adaptation to new host species. RNPs are composed of the viral genome, viral polymerase and many copies of the viral nucleoprotein. In vitro cell expression of all RNP protein components with four of the eight influenza virus gene segments enabled structural determination of native influenza virus RNPs by cryo-electron microscopy. The cryo-EM structure reveals the architecture and organization of the native RNP, thereby defining the attributes of its largely helical structure and how polymerase interacts with NP and the viral genome. Observations of branched-RNP structures in negative stain EM and their putative identification as replication intermediates suggest a mechanism for viral replication by a second polymerase on the RNP template.

Influenza A virus is a single-stranded RNA virus that causes frequent epidemics as well as sporadic pandemics (1). The constant threat of pandemic influenza is highlighted by the emergence of novel pandemic H1N1 viruses in 2009 (2) and the potential for highly pathogenic avian H5N1 viruses to gain human-to-human transmissibility (3). Several studies on influenza virus have pointed to components of the ribonucleoprotein complex (RNP) as key factors in host adaptation (4). The RNPs are responsible for viral transcription and replication as well as assembly of the genome segments into progeny virions (1).

The RNP is comprised of a single polymerase bound to the complementary RNA termini and multiple copies of the viral nucleoprotein (NP) that decorate the length of each of the eight single-stranded viral genome segments such that the RNP resembles a large loop, twisted into a helical filament (5). The RNA polymerase is composed of PB1, the catalytic subunit, and PB2 and PA subunits, which carry activities for priming transcription (1, 6, 7). Some fragment crystal structures have been determined (8), but how the subunits form a functional polymerase, interact with NP and the viral genome, or modulate interactions with host factors is still unclear.

Oligomerization of NP into a non-physiologic trimer, as observed in crystal structures, is facilitated by insertion of a long `tail-loop' from each NP monomer into a binding site on the adjacent monomer (9). The `tail-loop' has been shown biochemically to be important for oligomerization of NP monomers within the RNP (10–12), but structural information on the

*Correspondence to: bcarr@scripps.edu; wilson@scripps.edu.
†These authors contributed equally to this work

The authors report no conflicts of interest.

native RNP has been lacking and it is unclear how the NPs form the helical filament structures that are characteristic of influenza virus RNPs (5) Electron microscopy studies have previously been performed on constrained mini-RNPs (10) via truncation of the RNA genome to 254 nucleotides. The mini-RNP is not expected to recapitulate all of the interactions of native RNP complexes, which contain 890–2,341 nucleotides, particularly in formation of native-like filaments. To address the plethora of biological questions surrounding the influenza virus RNP, we used cryo-EM to analyze the structure of recombinant RNPs.

The RNPs were derived from influenza virus gene segments 1, 2, 3 and 5, which encode the protein components of the RNP complex, using a plasmid-based system (13). The co-expression of RNP protein components with viral genomes facilitates in vivo assembly of native RNP complexes with viral transcription and replication activity. The RNPs in the electron micrographs are highly flexible along their length (fig. S1), but display a regular diameter and repeat allowing 3-D reconstruction of the three main regions: the RNA-polymerase end, the central filament, and the looped-end (Fig. 1A,B, table S1) (5, 14).

Reconstruction of the central filament region was performed by selecting short, overlapping regions along the length of the RNP and applying helical symmetry based on initial analysis of non-symmetrized reconstructions. To reconstruct both ends of the RNP, putative RNP end regions (blunt and loop ends) were identified, selected and subsequently classified using a 3-D maximum likelihood approach (15, 16) to separate images of the loop end from the polymerase end. A polymerase in isolation reconstruction was obtained by digesting and disassembling the RNPs with ribonuclease. The 3-D maps are low-pass filtered at a resolution indicated by the Fourier shell coefficient curve at 0.5. Back projections of all 3-D reconstructions are in good agreement with their corresponding 2-D class averages (fig. S2–S5).

The 3-D cryo-EM reconstruction of a 23 nm segment of the central region of the RNP filament at 21 Å resolution (Fig. 1C) indicates that the NP-RNA complex forms two antiparallel strands that twist about one another to and from the RNA polymerase, which is bound to the RNA termini (5). Single NP protomers derived from the crystal structure (9) were fit into the EM map with the aid of automated docking procedures using structural, biological, and symmetry constraints (17) (Fig. 1D and movie S1). Influenza virus is unusual among RNA viruses in that transcription and replication occur within the cell nucleus (1). In the fitted model, the NP N-terminal nuclear localization signal (NLS I) is exposed, whereas a second putative NLS (NLS II) is buried in the protein-protein interface (fig. S6), in agreement with antibody labeling studies (18). While the modest resolution map does not allow an atomic interpretation, the protomer arrangement and regions of the NP can be localized within the RNP. The model is consistent with the finding (19) that the NP `tail-loop' is used for oligomerization along the NP-RNA strand (fig. S6) and the loss of transcriptional activity when residues in the NP `tail-loop' are mutated (fig. S7) (10–12). The RNP helix is stabilized by one NP-RNA strand interacting with the antiparallel NP-RNA strand near the NP head domains (fig. S8) (20). The NP orientation also directs the proposed NP RNA-binding regions into the inter-strand NP-NP interface such that the RNA sequences that are most intimately bound by NP are not directly accessible for transcription or replication, and suggests that at least local disassembly of the RNP is required for these processes to occur.

In this central region, adjacent NP protomers rise by 32.6 Å and twist by 73.9°, for an average of 4.9 NP along the RNA strand in one turn of the helix (21). The average periodicity of NP on the genomic RNA is 32 ribonucleotides (22) similar to the 26–32 nucleotide periodicity range calculated previously from constrained mini-RNP (10, 23, 24).

The average NP binding periodicity of the native RNP is understandably somewhat larger due to its more relaxed conformation. Furthermore, the spacing of the NP RNA-binding sites leaves large sections of RNA exposed (fig. S9), explaining the susceptibility of influenza virus RNP to ribonucleases (5). Some of the exposed RNA may present terminal genome assembly signals to facilitate interactions with the other gene segments and the assembly of the viral genome into progeny virions (25). These signals would be presented within about six NP, or 19 nm, from the polymerase end of the RNP, in agreement with recent influenza virus tomographic studies where interactions between the assembled eight RNPs are observed within 13–17 nm of the RNP filament end (26, 27).

The loop-end of the RNP was reconstructed from cryo-EM images to a resolution of approximately 40 Å and demonstrates that the NP-RNA strand makes a sharp U-turn to and from the central filament region (Fig. 1A and fig. S10). 2-D averages of negatively stained RNP show the loop is comprised of 5–8 NP monomers. The observed variation is likely due to different degrees of unwinding of the central filament region.

The polymerase-bound blunt end of the RNP was reconstructed to a resolution of 20 Å from the cryo-EM images. The heterotrimeric RNA-dependent RNA polymerase has two primary domains: a large domain and a smaller arm domain. Polymerase directly contacts two NPs on its large domain (Fig. 2A and fig. S10) and is adjacent to an additional NP monomer. Our reconstruction is similar to previously published densities (10); however, we identify a mass previously assigned to polymerase as more likely representing the adjacent additional NP monomer (fig S11). The structure of purified polymerase was determined by cryo-electron microscopy to 13 Å resolution (28). This higher-resolution structure could be fitted into the native RNP-bound polymerase reconstruction after rearrangement of the arm domain (Fig. 2B). Conformational isomerism of the arm domain is consistent with observations made for polymerases of other segmented negative-sense RNA viruses (29) (fig. S12). The arm domain is of a size and shape that suggests it is the PA C-terminal domain (30).

To locate the PB2 polymerase subunit within the RNP complex, the C terminus of the PB2 polymerase subunit in RNPs was labeled with 5 nm Nanogold and negatively stained. The gold label localizes to the base of the polymerase large domain near the contact site of the NP antiparallel helical screw (Fig. 2C). The PB2 `627' domain is located adjacent to the PB2 C terminus (31). Avian viruses lacking adaptive mutations on the surface of this domain, particularly Glu627Lys, are inhibited by a mammalian host factor that interferes with association of the avian polymerase with NP (32–34). Our identification of the `627' domain near the NP binding site on polymerase suggests a direct competition for polymerase binding between NP and the mammalian inhibitory host factor leading to host restriction for most avian viruses.

The NP protomers can be used as markers of the viral RNA genome path near the polymerase, as the viral RNA is not observable at the resolution of our reconstruction. One NP-RNA strand contacts polymerase near the PB2 C terminus, whereas the second NP-RNA strand departs from the helical filament to loop around and then contact polymerase via the PA C-terminal domain (fig. S10). This organization places the second RNA strand on the putative RNA binding site of the PA-CTD (30). Arg566Glu or Lys574Glu mutations in this binding site completely abolish transcriptional activity (fig. S7). Structural homology of the PA-CTD with the N-terminal domain of reovirus RNA polymerase (30, 35) suggests that this second strand is the 3′ end of the genome, which is directed towards the polymerase active site on the polymerase large domain; therefore, the first strand is the 5′ end (fig S13). The partially base-paired RNA termini must be proximal to the polymerase active site to place a 5′ proximal polyuridine stretch across the active site while remaining bound to the 5′ terminus and facilitate the proposed `stuttering' mechanism of polyadenylation (36) (Fig.

3A). The placement of the complementary RNA termini on the upper portion of the polymerase large domain is supported by a previous reconstruction of the polymerase bound to small RNA (37). These data support a model of RNA synthesis where PA-CTD plays a role in feeding template RNA into the polymerase active site.

Based on our structural models and incorporating additional structural and biochemical results from the literature, we can propose a model for viral transcription from influenza virus RNPs (Fig. 3B, fig. S14, and movie S2). In the pre-initiation state, the RNA termini are base paired adjacent to the polymerase active site. The PA and PB2 subunits bind and cleave host mRNA to produce capped primers for transcription initiation. The 3′ end then disengages from the 5′ end and repositions to the polymerase active site. As transcription proceeds, the PA-CTD moves single-stranded RNA from the RNP filament into the active site. As transcription reaches the 5′ end of the template and the RNA noose tightens, the 5′ terminus remains bound to the polymerase, positioning the polyuridine stretch across the active site. The polymerase stutters across this region to bring about polyadenylation and transcription termination.

Replication of the influenza virus genome is distinct from transcription in that the RNA product is not capped or polyadenylated. Viral replication involves the production of an intermediate cRNP complex composed of complementary RNA, polymerase and NP. The cRNP then acts as a template for viral genome synthesis. During replication, the RNP is thought to act only as a template with RNA polymerization carried out by a second polymerase (38). Examination of negative stain EM micrographs reveals numerous RNP complexes with a branched arrangement where a smaller nascent RNP appears to bud from a larger full-length RNP (Fig. 4). Nascent RNPs with very small lengths, half-length, or near full length are most common near the RNP filament ends as expected for a nascent RNP replicating on a full-length RNP template (fig. S15). Additionally, in RNP samples containing labeled polymerase, we observe polymerase residing at the junction of the smaller RNP with the full-length RNP (fig. S16). The observation of branched RNPs and their putative identification as replication intermediates is consistent with previous biochemical and structural investigation of vesicular stomatitis virus RNPs isolated from infected cells (39). These data support a model of influenza virus replication where a second polymerase acts on a template RNP leading to the formation of nascent RNP complexes concurrent with viral replication. It remains unclear how the second polymerase initiates replication. However, in our model, as replication proceeds, a new 5′ end is synthesized and is bound by the second replicating polymerase (Fig. 3C, fig. S17, movie S3). After 5′ terminus binding, the first NP protomer is added to the product RNA adjacent to the replicating polymerase's PB2 `627' domain initiating encapsidation of the viral genome or cRNA in a 5′ to 3′ direction and forming a nascent RNP on the template RNP giving the complex its branched appearance (Fig. 3C). This model describes NP encapsidation of the viral genome being initiated by sequence-specific binding of polymerase to the RNA 5′ end (40), concurrent with viral replication, which would account for NP encapsidation of viral RNA and not host RNA during viral infection.

These studies provide new insights into influenza virus transcription, replication, and host species adaptation and shed light on RNP nuclear translocation and virus assembly. These findings also suggest that the PB2-NP interaction and the PA-CTD conformational rearrangement are potential targets for novel therapeutics and demonstrate the utility of targeting the NP `tail-loop' binding site (12). Our model also provides a framework to develop new hypotheses to address how viral proteins and host factors interact with RNP for nuclear export and localization to the plasma membrane for virus assembly.

Supplementary Material

Refer to Web version on PubMed Central for supplementary material.

Acknowledgments

We thank R. Webster (St. Jude Children's Research Hospital) for providing the eight plasmid system (pHW2000, the cloning vector: pHW191-PB2, pHW192-PB1, pHW193-PA, and pHW195-NP, under an MTA from St. Jude) used for recombinant RNP expression, M. Brimble and P. Harris (Maurice Wilkins Centre for Molecular Biodiscovery, Univ. Auckland) for synthesizing the FLAG peptide, J. Quispe for help in EM grid specimen preparation, and A. Su for helpful advice on statistical analyses. We also thank J. Martín-Benito and J. Ortín (CSIC, Spain) for sending us the previously reconstructed mini-RNP map. This project has been funded in part by the National Institutes of Health AI058113 to I.A.W. and GM095573 to C.S.P and B.C. The project was also supported by grants from the National Center for Research Resources (2P41RR017573-11) and the National Institute of General Medical Sciences Biomedical Technology Resource Centers (9 P41 GM103310-11), and by the Joint Center for Innovation in Membrane Protein Production for Structure Determination (P50GM073197). This is publication 21687 from The Scripps Research Institute. The data presented in this manuscript are tabulated in the main paper and in the supplementary materials. Reconstructions of the free polymerase, RNP-bound polymerase, central filament and loop regions have been deposited in the Electron Microscopy Data Bank (EMDB entry numbers 2209, 2211, 2212, 2213). Coordinates of NP-protomers docked into the central filament map have been deposited in the Protein Data Bank (PDB code 2YMN)

References and Notes

1. Fields, BN.; Knipe, DM.; Howley, PM. Fields' Virology. Wolters Kluwer Health/Lippincott Williams & Wilkins; 2007.
2. Neumann G, Noda T, Kawaoka Y. Emergence and pandemic potential of swine-origin H1N1 influenza virus. Nature. 2009; 459:931–939. [PubMed: 19525932]
3. Hatta M, Gao P, Halfmann P, Kawaoka Y. Molecular basis for high virulence of Hong Kong H5N1 influenza A viruses. Science. 2001; 293:1840–1842. [PubMed: 11546875]
4. Gabriel G, et al. The viral polymerase mediates adaptation of an avian influenza virus to a mammalian host. Proc. Natl. Acad. Sci. USA. 2005; 102:18590–18595. [PubMed: 16339318]
5. Compans RW, Content J, Duesberg PH. Structure of the ribonucleoprotein of influenza virus. J. Virol. 1972; 10:795–800. [PubMed: 4117350]
6. Guilligay D, et al. The structural basis for cap binding by influenza virus polymerase subunit PB2. Nat. Struct. Mol. Biol. 2008; 15:500–506. [PubMed: 18454157]
7. Yuan P, et al. Crystal structure of an avian influenza polymerase PA_N reveals an endonuclease active site. Nature. 2009; 458:909–913. [PubMed: 19194458]
8. Ruigrok RW, Crepin T, Hart DJ, Cusack S. Towards an atomic resolution understanding of the influenza virus replication machinery. Curr. Opin. Struct. Biol. 2009; 20:104–113. [PubMed: 20061134]
9. Ng AK, et al. Structure of the influenza virus A H5N1 nucleoprotein: implications for RNA binding, oligomerization, and vaccine design. FASEB J. 2008; 22:3638–3647. [PubMed: 18614582]
10. Coloma R, et al. The structure of a biologically active influenza virus ribonucleoprotein complex. PLoS Pathog. 2009; 5:e1000491. [PubMed: 19557158]
11. Li Z, et al. Mutational analysis of conserved amino acids in the influenza A virus nucleoprotein. J. Virol. 2009; 83:4153–4162. [PubMed: 19225007]
12. Shen YF, et al. E339…R416 salt bridge of nucleoprotein as a feasible target for influenza virus inhibitors. Proc. Natl. Acad. Sci. USA. 2011; 108:16515–16520. [PubMed: 21930946]
13. Hoffmann E, Neumann G, Kawaoka Y, Hobom G, Webster RG. A DNA transfection system for generation of influenza A virus from eight plasmids. Proc. Natl. Acad. Sci. USA. 2000; 97:6108–6113. [PubMed: 10801978]
14. Materials and methods for particle expression and image analysis are available as supplementary information on *Science* Online
15. Sorzano CO, et al. XMIPP: a new generation of an open-source image processing package for electron microscopy. J. Struct. Biol. 2004; 148:194–204. [PubMed: 15477099]

16. Scheres SH, et al. Maximum-likelihood multi-reference refinement for electron microscopy images. J. Mol. Biol. 2005; 348:139–149. [PubMed: 15808859]
17. Pettersen EF, et al. UCSF Chimera--a visualization system for exploratory research and analysis. J. Comput. Chem. 2004; 25:1605–1612. [PubMed: 15264254]
18. Wu WW, Weaver LL, Pante N. Ultrastructural analysis of the nuclear localization sequences on influenza A ribonucleoprotein complexes. J. Mol. Biol. 2007; 374:910–916. [PubMed: 17976646]
19. Ye Q, Krug RM, Tao YJ. The mechanism by which influenza A virus nucleoprotein forms oligomers and binds RNA. Nature. 2006; 444:1078–1082. [PubMed: 17151603]
20. Mutations in the head domain interfaces did not show defects in transcriptional activity (fig. S7). However mutation of the helical strand interface results in defective RNP assembly (fig. S8). These results are consistent with previous work where NP mutants in this region retained wild-type transcription activity in mini-genome assays, but could not be rescued as virus (11)
21. Given the slight variations in RNP helical rise and twist, reported helical parameters likely represent average values.
22. The 32 nucleotide NP periodicity was calculated from an RNA segment length of approximately 2,300 nucleotides and a total of 69 NP within the RNP, which was estimated from the end region reconstructions, the helical rise (3.26 nm), and total RNP length (110 nm).
23. Ortega J, et al. Ultrastructural and functional analyses of recombinant influenza virus ribonucleoproteins suggest dimerization of nucleoprotein during virus amplification. J. Virol. 2000; 74:156–163. [PubMed: 10590102]
24. The 26–32 nucleotide periodicity of NP binding is calculated from (23) and is based on mini-RNPs having a 350 nucleotide genome bound to 10-12 NP.
25. Hutchinson EC, von Kirchbach JC, Gog JR, Digard P. Genome packaging in influenza A virus. J. Gen. Virol. 2010; 91:313–328. [PubMed: 19955561]
26. Fournier E, et al. A supramolecular assembly formed by influenza A virus genomic RNA segments. Nucleic Acids Res. 2012; 40:2197–2209. [PubMed: 22075989]
27. Noda T, et al. Three-dimensional analysis of ribonucleoprotein complexes in influenza A virus. Nat. Commun. 2012; 3:639. [PubMed: 22273677]
28. The density is similar to that published earlier at lower resolution (41). The previously noted large cleft in the polymerase resolves into a space between the polymerase large and arm domains (fig. S12).
29. Kranzusch PJ, et al. Assembly of a functional Machupo virus polymerase complex. Proc. Natl. Acad. Sci. USA. 2010; 107:20069–20074. [PubMed: 20978208]
30. He X, et al. Crystal structure of the polymerase PA_C-$PB1_N$ complex from an avian influenza H5N1 virus. Nature. 2008; 454:1123–1126. [PubMed: 18615018]
31. Tarendeau F, et al. Host determinant residue lysine 627 lies on the surface of a discrete, folded domain of influenza virus polymerase PB2 subunit. PLoS Pathog. 2008; 4:e1000136. [PubMed: 18769709]
32. Labadie K, Dos Santos Afonso E, Rameix-Welti MA, van der Werf S, Naffakh N. Host-range determinants on the PB2 protein of influenza A viruses control the interaction between the viral polymerase and nucleoprotein in human cells. Virology. 2007; 362:271–282. [PubMed: 17270230]
33. Mehle A, Doudna JA. An inhibitory activity in human cells restricts the function of an avian-like influenza virus polymerase. Cell Host Microbe. 2008; 4:111–122. [PubMed: 18692771]
34. Rameix-Welti MA, Tomoiu A, Dos Santos Afonso E, van der Werf S, Naffakh N. Avian Influenza A virus polymerase association with nucleoprotein, but not polymerase assembly, is impaired in human cells during the course of infection. J. Virol. 2009; 83:1320–1331. [PubMed: 19019950]
35. Tao Y, Farsetta DL, Nibert ML, Harrison SC. RNA synthesis in a cage -- structural studies of reovirus polymerase λ3. Cell. 2002; 111:733–745. [PubMed: 12464184]
36. Luo GX, Luytjes W, Enami M, Palese P. The polyadenylation signal of influenza virus RNA involves a stretch of uridines followed by the RNA duplex of the panhandle structure. J. Virol. 1991; 65:2861–2867. [PubMed: 2033659]
37. Resa-Infante P, Recuero-Checa MA, Zamarreno N, Llorca O, Ortin J. Structural and functional characterization of an influenza virus RNA polymerase-genomic RNA complex. J. Virol. 2012; 84:10477–10487. [PubMed: 20702645]

38. Jorba N, Coloma R, Ortin J. Genetic trans-complementation establishes a new model for influenza virus RNA transcription and replication. PLoS Pathog. 2009; 5:e1000462. [PubMed: 19478885]
39. Naeve CW, Summers DF. Electron microscopy of vesicular stomatitis virus replicative ribonucleoproteins. J Virol. 1980; 34:764–771. [PubMed: 6247510]
40. Baudin F, Bach C, Cusack S, Ruigrok RW. Structure of influenza virus RNP. I. Influenza virus nucleoprotein melts secondary structure in panhandle RNA and exposes the bases to the solvent. EMBO J. 1994; 13:3158–3165. [PubMed: 8039508]
41. Torreira E, et al. Three-dimensional model for the isolated recombinant influenza virus polymerase heterotrimer. Nucleic Acids Res. 2007; 35:3774–3783. [PubMed: 17517766]
42. Klock HE, Lesley SA. The Polymerase Incomplete Primer Extension (PIPE) method applied to high-throughput cloning and site-directed mutagenesis. Methods Mol. Biol. 2009; 498:91–103. [PubMed: 18988020]
43. Ruigrok RW, Baudin F. Structure of influenza virus ribonucleoprotein particles. II. Purified RNA-free influenza virus ribonucleoprotein forms structures that are indistinguishable from the intact influenza virus ribonucleoprotein particles. J. Gen. Virol. 1995; 76:1009–1014. [PubMed: 9049350]
44. Suloway C, et al. Automated molecular microscopy: the new Leginon system. J. Struct. Biol. 2005; 151:41–60. [PubMed: 15890530]
45. Lander GC, et al. Appion: an integrated, database-driven pipeline to facilitate EM image processing. J. Struct. Biol. 2009; 166:95–102. [PubMed: 19263523]
46. Mindell JA, Grigorieff N. Accurate determination of local defocus and specimen tilt in electron microscopy. J. Struct. Biol. 2003; 142:334–347. [PubMed: 12781660]
47. Roseman AM. FindEM--a fast, efficient program for automatic selection of particles from electron micrographs. J. Struct. Biol. 2004; 145:91–99. [PubMed: 15065677]
48. Voss NR, Yoshioka CK, Radermacher M, Potter CS, Carragher B. DoG Picker and TiltPicker: software tools to facilitate particle selection in single particle electron microscopy. J. Struct. Biol. 2009; 166:205–213. [PubMed: 19374019]
49. van Heel M, Harauz G, Orlova EV, Schmidt R, Schatz M. A new generation of the IMAGIC image processing system. J. Struct. Biol. 1996; 116:17–24. [PubMed: 8742718]
50. Scheres SH, Nunez-Ramirez R, Sorzano CO, Carazo JM, Marabini R. Image processing for electron microscopy single-particle analysis using XMIPP. Nat. Protoc. 2008; 3:977–990. [PubMed: 18536645]
51. Radermacher M, Wagenknecht T, Verschoor A, Frank J. A new 3-D reconstruction scheme applied to the 50S ribosomal subunit of E. coli. J. Microsc. 1986; 141:RP1–2. [PubMed: 3514918]
52. Fisher LS, et al. A helical processing pipeline for EM structure determination of membrane proteins. Methods. 2011; 55:350–362. [PubMed: 21964395]
53. Egelman EH. Single-particle reconstruction from EM images of helical filaments. Curr. Opin. Struct. Biol. 2007; 17:556–561. [PubMed: 17851070]
54. Parent KN, et al. Cryo-reconstructions of P22 polyheads suggest that phage assembly is nucleated by trimeric interactions among coat proteins. Phys. Biol. 2010; 7:045004. [PubMed: 21149969]
55. Scheres SH, Valle M, Carazo JM. Fast maximum-likelihood refinement of electron microscopy images. Bioinformatics. 2005; 21:ii243–244. [PubMed: 16204112]
56. Frank J, et al. SPIDER and WEB: processing and visualization of images in 3D electron microscopy and related fields. J. Struct. Biol. 1996; 116:190–199. [PubMed: 8742743]
57. Marjuki H, et al. Higher polymerase activity of a human influenza virus enhances activation of the hemagglutinin-induced Raf/MEK/ERK signal cascade. Virol. J. 2007; 4:134–152. [PubMed: 18053252]
58. Zhu W, et al. A reporter system for assaying influenza virus RNP functionality based on secreted Gaussia luciferase activity. Virol. J. 2011; 8:29–35. [PubMed: 21251302]

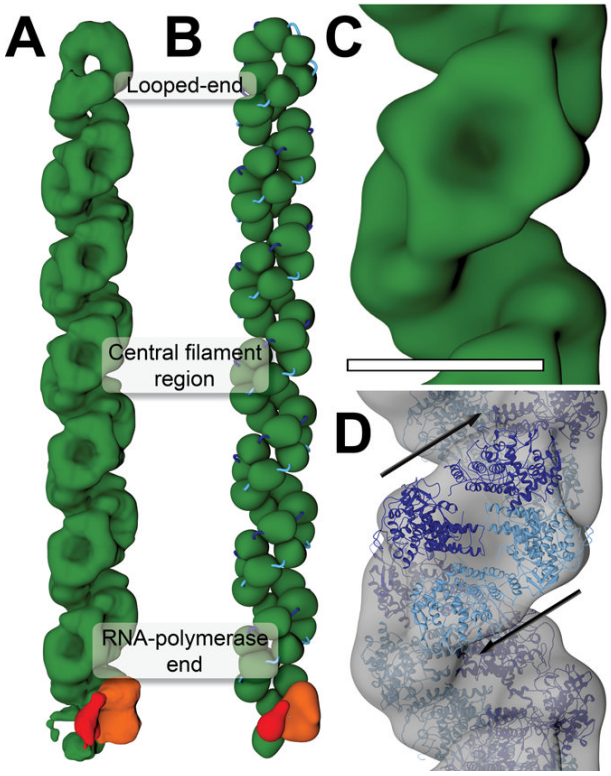

Fig. 1. Cryo-EM reconstruction of the influenza virus ribonucleoprotein complex

(A) Composite model of cryo-EM reconstructions of the three regions of the RNP. (**B**) Cartoon representation of the RNP organization. The large domain of polymerase is shown in orange with the arm domain in red. Nucleoproteins are shown in green and RNA in blue. (**C**) Reconstruction of the central filament region using helical symmetry. (**D**) Single protomers from the NP crystal structure (*9*) were fitted into the EM density. The arrangement of the NP (light-blue for descending strand and dark blue for ascending strand) within the filament creates a periodic box type arrangement formed from four NPs with a region of low density or dimple in the center of the box. This box-like feature is also easily identifiable in our reconstructions of the loop and polymerase end regions. Arrows indicate RNA polarity. Scale bar represents 10 nm.

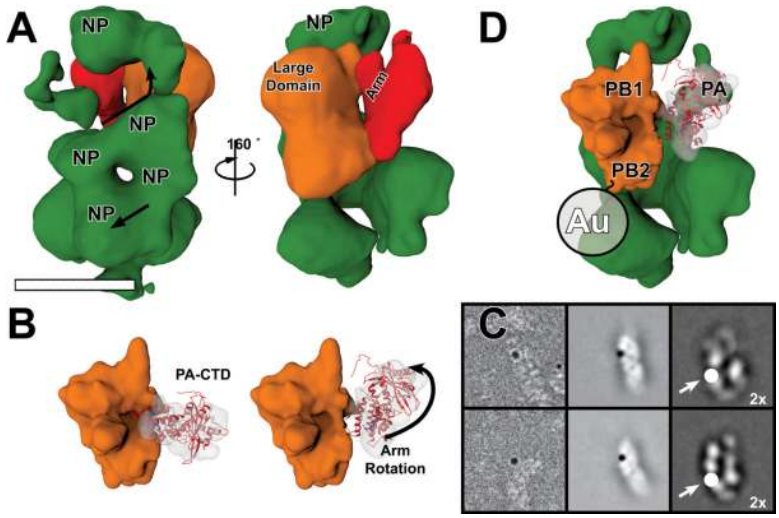

Fig. 2. The influenza virus RNA polymerase and its interactions at the RNP terminus

(A) The RNP-bound polymerase large domain (orange) caps the central RNP filament region. A single NP from the second strand that has emerged from the central filament follows the 3′ RNA strand as it loops behind polymerase to contact the PA CTD (red). (**B**) Cryo-EM reconstruction of the free polymerase (left) shows it consists of a large domain (orange) and an arm containing the PA CTD (red) (*30*). The arm domain conformation in the RNP is accommodated by a rotation about a pivot near the base of the arm (right). (**C**) 2-D averages and raw images of negatively stained RNPs labeled with 5 nm Nanogold (upper and middle panels respectively) localize the PB2 C terminus to the bottom of the large domain near the NP contact site. The lower panels show 2-D projections of 21 Å RNP-bound polymerase with an additional circle (indicated with an arrow) below the polymerase-large domain corresponding to the size of the 5 nm Nanogold for comparison with labeled 2-D class averages. (**D**) The composite image of the RNP polymerase end has been labeled to indicate putative subunit locations based on the PA CTD docking, Nanogold labeling of the PB2 C-terminus and structural homology with reovirus polymerase. The location of the 5 nm Nanogold labeling the PB2 C-terminus is shown as a circle labeled Au. Because the reconstruction is centered on the polymerase and the RNP is flexible, additional density corresponding to distal regions of poorly aligned RNP filaments is visible beneath the well-ordered components.

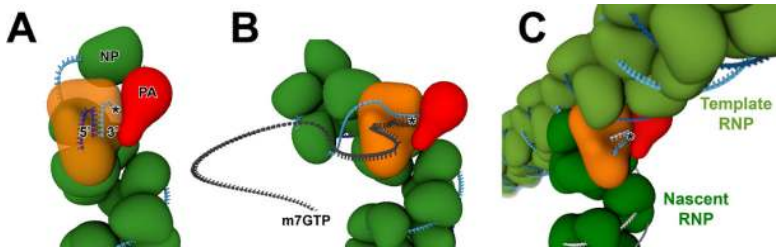

Fig. 3. Models for influenza virus RNA synthesis

(A) In the resting RNP, polymerase is bound to both 5′ and 3′ termini, as would be expected in virions. The polymerase large domain and arm domain are colored orange and red respectively. The nucleoprotein is in green and the genomic RNA is in light blue for 3′ end and dark blue for the 5′ end. The active site (*) and RNA polarity were identified using structural homology with the reovirus λ3 polymerase (fig S13). (**B**) Viral transcription of mRNA is carried out by the resident polymerase acting. In this process, template RNA is pulled up from beneath polymerase, passed through the active site where it is transcribed into capped mRNA (black) and then re-encapsidated into a NP-RNA complex, which coils up to form an RNP-like structure. (**C**) Replication of viral RNA is carried out by a second polymerase leading to nascent RNP formation. The second replicating polymerase binds a newly synthesized 5′ end and initiates encapsidation of the viral genome by NP in a 5′ to 3′ manner leading to nascent RNP formation.

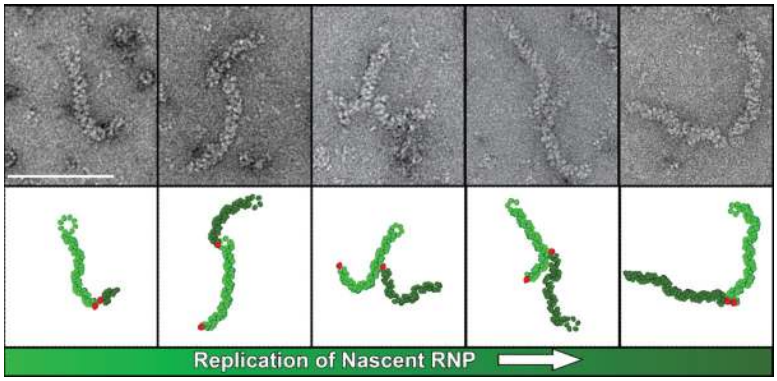

Fig. 4. Formation of nascent RNP during replication. (Upper panel)
Electron micrographs of the negatively stained RNP sample at high dilution reveal branched RNPs predicted to be replication intermediates. (**Lower panel**) Interpretation of the branched RNPs in the upper panel showing how replication of the viral RNA *in trans* by a second polymerase (red) could result in nascent RNP complexes (dark green) branching from the template RNP (light green). As the nascent RNP moves away from and then back towards the template RNP polymerase, that is, 3′ to 5′ along the genomic template, it would elongate the complementary RNA and extends its length. Scale bar corresponds to 100 nm.